catalysts

MDPI

Article

The Support Effects on the Direct Conversion of Syngas to Higher Alcohol Synthesis over Copper-Based Catalysts

Xiaoli Li [1,2], Junfeng Zhang [1], Min Zhang [3], Wei Zhang [3], Meng Zhang [1,2], Hongjuan Xie [1], Yingquan Wu [1] and Yisheng Tan [1,4,*]

1 State Key Laboratory of Coal Conversion, Institute of Coal Chemistry, Chinese Academy of Sciences, Taiyuan 030001, China; lixiaoli@sxicc.ac.cn (X.L.); zhangjf@sxicc.ac.cn (J.Z.); zhangmeng@sxicc.ac.cn (M.Z.); xiehj@sxicc.ac.cn (H.X.); wuyq@sxicc.ac.cn (Y.W.)
2 School of Chemical Science, University of Chinese Academy of Sciences, Beijing 100049, China
3 Technology Center, Shanxi Lu'an Mining (Group) Co. Ltd., Changzhi 046204, China; zmin925@163.com (M.Z.); 15934381920@163.com (W.Z.)
4 National Engineering Research Center for Coal-Based Synthesis, Institute of Coal Chemistry, Chinese Academy of Sciences, Taiyuan 030001, China
* Correspondence: tan@sxicc.ac.cn; Tel./Fax: +86-351-404-4287; +86-351-404-4287

Received: 21 January 2019; Accepted: 9 February 2019; Published: 21 February 2019

Abstract: The types of supports employed profoundly influence the physicochemical properties and performances of as-prepared catalysts in almost all catalytic systems. Herein, Cu catalysts, with different supports (SiO_2, Al_2O_3), were prepared by a facile impregnation method and used for the direct synthesis of higher alcohols from CO hydrogenation. The prepared catalysts were characterized using multiple techniques, such as X-ray diffraction (XRD), N_2 sorption, H_2-temperature-programmed reduction (H_2-TPR), temperature-programmed desorption of ammonia (NH_3-TPD), X-ray photoelectron spectroscopy (XPS) and in situ Fourier-transform infrared spectroscopy (FTIR), etc. Compared to the Cu/Al_2O_3 catalyst, the Cu/SiO_2 catalyst easily promoted the formation of a higher amount of C1 oxygenate species on the surface, which is closely related to the formation of higher alcohols. Simultaneously, the Cu/Al_2O_3 and Cu/SiO_2 catalysts showed obvious differences in the CO conversion, alcohol distribution, and CO_2 selectivity, which were probably originated from differences in the structural and physicochemical properties, such as the types of copper species, the reduction behaviors, acidity, and electronic properties. Besides, it was also found that the gap in performances in two kinds of catalysts with the different supports could be narrowed by the addition of potassium because of its neutralization to surface acidy of Al_2O_3 and the creation of new basic sites, as well as the alteration of electronic properties.

Keywords: CO hydrogenation; higher alcohols; support effects; Cu-based catalysts

1. Introduction

Higher alcohols are attracting considerable attentions owing to their broad applications, such as fuels, fuel additives, and feedstock for the production of various chemicals and polymers [1–3]. With increasing concerns for environmental pollution and depletion of non-renewable petroleum resources, there is a growing interest in the direct synthesis of oxygenates, especially higher alcohols synthesis via syngas derived from coal, natural gas, or biomass [4]. Generally, the catalysts suitable for higher alcohols synthesis can be divided into the following classes: (I) Rh-based catalysts [5,6], (II) the modified Fischer–Tropsch catalysts [7,8], (III) Mo-based catalysts [9], and (IV) the modified Cu-based catalysts for methanol synthesis [10–14]. Non-noble Cu-based catalysts, due to their

comparable high activity, are regarded as one kind of the most promising candidates for higher alcohols synthesis [4,13,15].

With respect to Cu-based catalysts, remarkably important advances have been made and reported owing to the simple preparation method and full utilization of active components [2,4,10–18]. It has been well documented that interaction between metal oxide and the support significantly improved the dispersion of the active species [19,20], stabilized active species [12], and promoted the generation of new inter-phases [16,17,21,22], thereby strongly influencing the catalytic performance [19–29]. Lemonidou et al. [19] compared the catalytic activities of the three Ni-Mo catalysts supported by activated carbon (AC), Al_2O_3, and ZrO_2, respectively. They revealed that the activity was closely related to the dispersion of the active phase on support surface, and AC support with a higher surface area was helpful for the exposure of more active Ni-O-Mo sites. Y. Khodakov et al. [20] found that Cu-Co supported on Al_2O_3, due to relatively high metal dispersion and formation of copper cobalt bimetallic species, exhibited much higher alcohol selectivity than that supported on other materials. Wang et al. [21] studied the Al_2O_3-supported Cu-Co bimetallic catalysts for CO hydrogenation and revealed that the employment of Al_2O_3 can significantly increase the interaction between cobalt and copper particles compared with unsupported catalysts, thereby improving the selectivity of the catalysts to higher alcohols. Lee et al. [23] investigated the effect of supports (ZnO, MgO, and Al_2O_3) on the activity of Cu-Co catalysts for the hydrogenation reaction of CO and suggested that the high surface area and strong interaction between active centers and support played a vital role in improving alcohol formation. By comparing the Cu-Zn catalysts with and without γ-Al_2O_3, Choi [30] et al. pointed out that the selectivity of higher alcohols and CO conversion over a Cu-Zn catalyst supported on γ-Al_2O_3 were higher than 1.8 and 2.7 times that of a Cu-Zn catalyst without γ-Al_2O_3, respectively. They further found that a refractory $CuAl_2O_4$, formed via the thermal reaction of CuO and Al^{3+}, was able to enhance the long-term stability by increasing the resistance to sintering of the catalyst. Sun et al. [31] studied methanol synthesis from CO_2 hydrogenation over micro-spherical SiO_2 support Cu/ZnO catalysts and found that the catalytic activity was enhanced as a result of the small Cu particle size and uniform metal dispersion. Co-Cu bimetallic catalysts with SiO_2 support have been thoroughly investigated for higher alcohols synthesis from syngas by Han et al [32]. It suggested that CoCu bimetallic particles covered by Cu atoms were responsible for alcohols synthesis. Ma et al. [22,33,34] reported that the improvement of Cu dispersion was mainly ascribed to the generation of copper phyllosilicate ($Cu_2SiO_5(OH)_2$) caused by enhanced metal-support interactions, which was quite vital for the high activity and stability in the ethanol synthesis. The above literature clearly showed that Al_2O_3 and SiO_2 are good support candidates to prepare the catalyst with good performance in the synthesis of higher alcohols.

Our group has also spent considerable effort to study the Al_2O_3 and SiO_2 supported Cu-based catalysts for the higher alcohols synthesis from syngas [12,16,17,35]. In our latest work, we found that the interaction between Cu and Al_2O_3 support on K-Cu/Al_2O_3 catalysts could be effectively tuned by changing the calcination temperature, which led to the different distribution of CuO, $CuAl_2O_4$, and $CuAlO_2$ on the catalysts and strongly affected the reaction behaviors in the direct synthesis of ethanol from syngas [16,17]. For the Cu catalyst with SiO_2 support, the correlation of catalyst structure evolution and ethanol selectivity during the reaction process was systematically discussed [35]. Although we had somewhat understood the relation between copper species and performance of the supported Cu-based catalysts, the direct comparison of Al_2O_3 and SiO_2 supported Cu catalysts and the effects of supports, treated at similar conditions, on the direct synthesis of higher alcohols from CO hydrogenation had not been sufficiently discussed.

Therefore, this work was mainly to clarify the reason of difference in reaction behaviors over the Cu catalysts supported on Al_2O_3 and SiO_2 for CO hydrogenation into higher alcohols. Considering that alkali addition strongly affected the selectivity towards higher alcohols [13,15,36–41], herein, the present study also put forth effort to explore the effects of potassium addition on the structure and performance of Al_2O_3 and SiO_2 supported Cu catalysts. Moreover, the physicochemical

properties of the prepared catalysts were characterized via various techniques, including X-ray diffraction (XRD), N_2 absorption-desorption, H_2-temperature-programmed reduction (H_2-TPR), temperature-programmed desorption of ammonia (NH_3-TPD), X-ray photoelectron spectroscopy (XPS), and in situ Fourier-transform infrared spectroscopy (FTIR), and the characterization results were discussed alongside with the catalytic data in detail.

2. Materials and Methods

2.1. Materials

Analytical-grade chemicals, including $Cu(NO_3)_2 \cdot \times 3H_2O$, NaOH, $AlCl_3 \cdot \times 6H_2O$, and K_2CO_3, were purchased from the Beijing Chemical Co. Ltd. (Beijing, China) and used directly without further purification. The employed SiO_2 was purchased from Aladdin Industrial Co. Ltd. (Los Angeles, US). The γ-Al_2O_3, as a support was synthesized using a hydrothermal route, which was similar to the procedure described by Yang et al. [42]. Typically, the ammonia solution (28% NH_3), $AlCl_3 \cdot \times 6H_2O$ solution, and NaOH solution were mixed under hydrothermal treatment. Then, the mixture was dried and calcined to obtain the γ-Al_2O_3.

2.2. The Preparation of Cu/Al_2O_3, $K\text{-}Cu/Al_2O_3$ and Cu/SiO_2, $K\text{-}Cu/SiO_2$ Catalysts

The Al_2O_3 and SiO_2 supports with a near Brunauer-Emmett-Teller (BET) surface area (157–160 m^2/g) were chosen in this study. The catalysts were prepared using a sequential impregnation method. Typically, for the Cu/Al_2O_3 and $K\text{-}Cu/Al_2O_3$ catalysts, 6.74 g of $Cu(NO_3)_2 \times 3H_2O$ (10 wt % CuO) was dissolved in 20 mL of deionized water. Twenty grams of Al_2O_3 were added into the above copper nitrate solution and impregnated by the ultrasonic treatment for 1 h at room temperature. Afterward, the mixture was dried at 120 °C for 10 h and calcined at 900 °C for 5 h in air. The obtained solid was Cu/Al_2O_3 catalyst. $K\text{-}Cu/Al_2O_3$ catalyst was prepared through the second impregnation of Cu/Al_2O_3 in K_2CO_3 aqueous solution. Simply, 0.61 g of K_2CO_3 (4 wt % K_2O loading) was dissolved in another 10 mL of deionized water. The desired amount of the Cu/Al_2O_3 catalyst obtained above was impregnated in K_2CO_3 aqueous solution, along with the ultrasonic treatment, for 1 h at room temperature. Then, the resulting mixture was dried at 120 °C for 10 h and calcined at 500 °C for 5 h in air. The Cu/SiO_2 and $K\text{-}Cu/SiO_2$ catalysts were also prepared using a method similar to one above. For comparison, the Al_2O_3 and SiO_2 supports were also calcined at 900 °C for 5 h in air and denoted as Al_2O_3-900 and SiO_2-900, respectively.

2.3. Catalyst Characterization

The textural properties of the as-prepared catalysts were measured with N_2 absorption-desorption at −196 °C on a Tristar 3000 Micromeritics (Atlanta, GA, US) instrument. The specific surface area (S_{BET}) was calculated by the BET method. The micropore volume was obtained from the t-plot method. The pore size distributions were evaluated by using the density functional theory (DFT) method applied to the nitrogen adsorption data. The measurement of textural properties is accuracy (±1%). The experiments were repeated three times.

Powder XRD patterns of the catalysts were collected on a Rigaku MiniFlex II X-ray diffractometer (Tokyo, Japan), using Ni-filtered Cu-Kα radiation (k = 0.15418 nm) with a scanning angle (2θ) of 10–90°.

H_2-TPR was carried out on an automatic temperature-programmed chemisorption analyzer (TP-5080, Tianjin Xianquan Industrial Trade and Develpment Co. Ltd, Tianjin, China) equipped with a thermal conductivity detector. The catalyst with 100 mg was pretreated at 300 °C under a flow of N_2 (32 mL/min) for 1 h to remove traces of water and then cooled to 50 °C. Subsequently, the gas flow was switched to a 10% H_2/N_2 (v/v, 35 mL/min). The sample was heated to 900 °C at a rate of 10 °C/min.

NH_3-TPD was carried out on a TP-5080 chemisorption instrument in order to evaluate the acidity of the catalysts. The catalyst (100 mg) was pretreated at 400 °C under a flow of N_2 (32 mL/min) for 1 h

and then cooled down to 100 °C. After that, sample was exposed on NH_3 flow for 15 min. The TPD spectra were recorded from 100 to 600 °C, using a heating rate of 10 °C/min.

Characterizations of XPS and Auger electron spectroscopy (XAES) were conducted on an AXIS ULTRA DLD instrument (Kratos, Manchester, UK) equipped with Al Kα (hν = 1486.6 eV). The binding energy values were corrected for charging effects by referring to the adventitious C1s line at 284.5 eV.

In situ FTIR spectra of CO adsorption and desorption were obtained with a TENSOR-27 in the range from 4000 to 1000 cm^{-1} with 4 cm^{-1} resolution. Before CO adsorption, all catalysts were reduced at 400 °C for 0.5 h in a 10% H_2/N_2 (v/v, 15 mL/min). CO adsorption was taken at 400 °C and after 30 min of pure Ar flow at the same temperature. IR spectra were collected after evacuation for 30 min.

2.4. Catalytic Performance Evaluation

The catalyst test of CO hydrogenation was performed in a stainless fixed-bed reactor. In a typical run, 5 mL of the prepared catalyst (30–40 meshes) was placed in the center of the reactor. The catalyst was reduced according to the designed temperature program, i.e., from room temperature to 400 °C in a 10% H_2/N_2 (v/v, 35 mL/min) mixture at 400 °C for 4 h. The reaction was conducted at 400 °C, 10 MPa and 5000 h^{-1}. The flow rate of fed syngas (with CO/H_2 ratio of 1 to 2.7) was controlled by a mass flow controller, and the exit gases were measured using a wet test meter. The products were analyzed using four chromatographs during the reaction. The organic gas products, consisting of hydrocarbons and methanol, were detected online on GC4000A (EastWest, Beijing, China) equipped with flame ionization detector and GDX-403 column (EastWest, Beijing, China) (3 mm, 1 m). The inorganic gas products were detected online by thermal conductivity measurements using an EastWest GC4000A (carbon molecular sieves column, 3 m, 3m). The H_2O and methanol products in the liquid phase were detected by thermal conductivity measurements using a GC4000A (Shimazduo, Kyoto, Japan) (GDX-401 column, Shimazduo, Kyoto, Japan, 3 mm, 3 m). The alcohol products in the liquid phase were detected by flame ionization measurements using a Shimazduo GC-7AG (Shimazduo, Kyoto, Japan) (Chromosorb 101, Shimazduo, Kyoto, Japan, 3 mm, 4 m).

3. Results and Discussion

3.1. Catalyst Characterization

3.1.1. XRD

The XRD patterns of Al_2O_3, Al_2O_3-900, Cu/Al_2O_3, K-Cu/Al_2O_3 catalysts (Figure 1a) and SiO_2, SiO_2-900, Cu/SiO_2, K-Cu/SiO_2 catalysts (Figure 1b) are shown in Figure 1. No obvious changes were observed in the XRD patterns of the supports (Al_2O_3 and SiO_2) before and after calcination, revealing that tuning calcination temperature did not influence the phases of the supports. In the case of the Cu/Al_2O_3 and Cu/SiO_2 catalysts, the XRD patterns were very different from that of the supports. Specifically, the diffraction peaks (2θ = 31.3, 39.4, 42.6, 52.5, and 55.7°) of the $CuAlO_2$ phase (JCPDS no. 39-0246) [43] and the peaks (2θ = 31.3, 36.9, 44.9, 55.7, 59.5, 65.3, 77.2, and 80.8°) of the $CuAl_2O_4$ phase (JCPDS no. 33-0448) [16,43] appeared in the Cu/Al_2O_3 catalysts (as shown in Figure 1a). Unlike the Cu/Al_2O_3 catalyst, the Cu/SiO_2 catalyst showed the peaks (2θ = 35.7 and 38.9°) of CuO phase (JCPDS no. 05-661) [22,44] and the peaks (2θ = 31.4, 57.5, and 62.4°) of copper phyllosilicate [33,34] (as displayed in Figure 1b). In addition, potassium introduction (such as the K-Cu/Al_2O_3 catalyst and the K-Cu/SiO_2 catalyst) did not seemingly induce obvious changes in the diffraction peaks. These findings clearly revealed that copper species reacted with the support to form new phases when calcined at 900 °C, and the supports strongly affected the forms of copper species, but the potassium had no obvious effect on the phases of the catalysts.

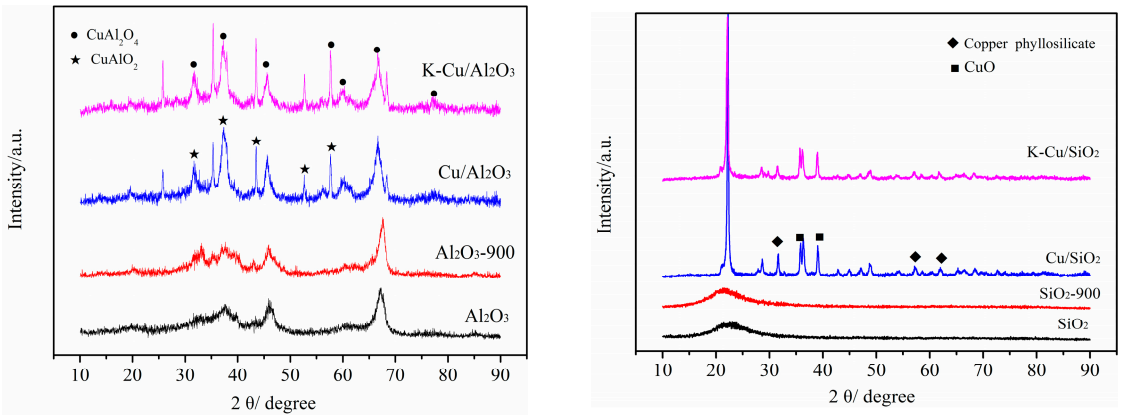

(**a**) (**b**)

Figure 1. X-ray diffraction (XRD) patterns of (**a**) Al_2O_3, Al_2O_3-900, Cu/Al_2O_3, K-Cu/Al_2O_3 catalysts and (**b**) SiO_2, SiO_2-900, Cu/SiO_2, K-Cu/SiO_2 catalysts.

3.1.2. N_2 Absorption-Desorption

The textural properties of the Al_2O_3, Al_2O_3-900, SiO_2, SiO_2-900, Cu/Al_2O_3, K-Cu/Al_2O_3 and Cu/SiO_2, K-Cu/SiO_2 catalysts were listed in Table 1. In comparison of the parent Al_2O_3 (157 m^2/g) and SiO_2 (160 m^2/g), the BET surface areas of Al_2O_3-900 and SiO_2-900 dramatically decreased to 87.0 and 25.8 m^2/g, respectively, via calcination at 900 °C, which was strongly associated with the collapse of porous structure during the high-temperature calcination process. In addition, when copper species were introduced into the uncalcined supports, the surface areas of the Cu/Al_2O_3 and Cu/SiO_2 catalysts sharply dropped to 41.6 and 6.69 m^2/g, which were much smaller than that of Al_2O_3-900 and SiO_2-900, respectively. The decrease in surface areas was probably due to both the formation of interfacial composite phases and copper as a sintering agent. As also shown in Table 1, compared with the Cu/Al_2O_3 and K-Cu/Al_2O_3 catalysts, the Cu/SiO_2 and K-Cu/SiO_2 catalysts showed considerably lower values of the surface area (4.63–6.69 m^2/g), smaller pore volume (0.006–0.008 cm^3/g), and average pore diameter (5.26–5.66 nm). When potassium was added, the surface area, pore volume, and average pore diameter of Al_2O_3 supported catalysts further decreased (from 41.6 to 40.7 m^2/g, 0.20 to 0.18 cm^3/g, and 19.1 to 17.8 nm, respectively). The surface areas and pore volume of SiO_2 supported catalysts also showed a decreasing trend (from 6.69 to 4.63 m^2/g and 0.008 to 0.006 cm^3/g, respectively), but the value of average pore diameter slightly increased from 5.26 to 5.66 nm, which was probably related to the corrosion of potassium to SiO_2. The results indicated that the textural parameters of the samples were greatly affected by both supports (Al_2O_3, SiO_2) and potassium.

Table 1. Textural properties of the representative samples.

Catalyst	S_{BET} (m^2/g)	V_{Pore} (cm^3/g)	d_{Pore} (nm)
Al_2O_3	157	0.43	10.8
Al_2O_3-900	87.0	0.39	18.1
Cu/Al_2O_3	41.6	0.20	19.1
K-Cu/Al_2O_3	40.7	0.18	17.8
SiO_2	160	0.54	13.7
SiO_2-900	25.8	0.07	10.6
Cu/SiO_2	6.69	0.008	5.26
K-Cu/SiO_2	4.63	0.006	5.66

The N_2 adsorption-desorption isotherms of the Cu/Al_2O_3, $K\text{-}Cu/Al_2O_3$ and Cu/SiO_2, $K\text{-}Cu/SiO_2$ catalysts were shown in Figure 2a. As observed, Cu/Al_2O_3 catalyst showed a type IV adsorption isotherm [9]. When potassium was added, the shape of the isotherms of Al_2O_3 supported catalysts did not change significantly. Unlike Al_2O_3 suppored catalysts, SiO_2 supported catalysts had no N_2 adsorption-desorption isotherms.

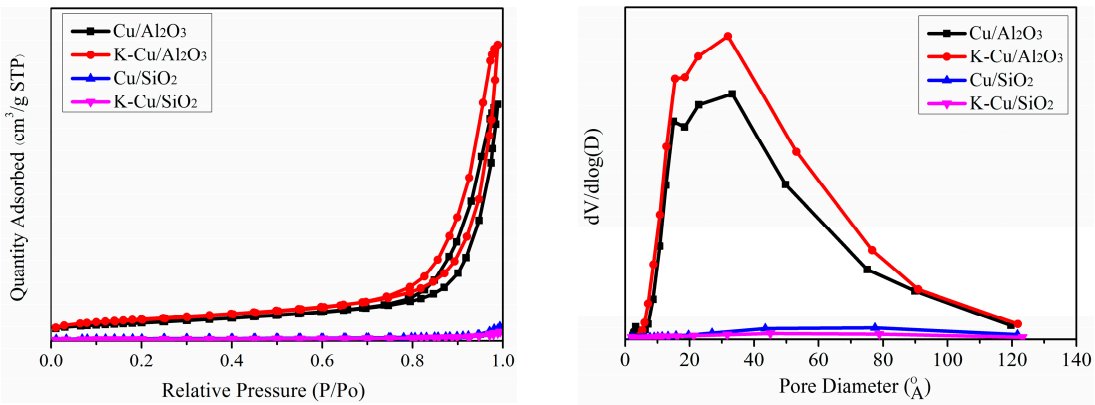

(**a**) (**b**)

Figure 2. (**a**) Nitrogen adsorption-desorption isotherms and (**b**) pore size distribution of Cu/Al_2O_3, $K\text{-}Cu/Al_2O_3$ and Cu/SiO_2, $K\text{-}Cu/SiO_2$ catalysts.

Figure 2b presented the pore size distribution curves of the Cu/Al_2O_3, $K\text{-}Cu/Al_2O_3$ and Cu/SiO_2, $K\text{-}Cu/SiO_2$ catalysts. It was clearly observed that the Cu/Al_2O_3 catalyst had a wide range of 10–120 Å, while the addition of potassium, such as the $K\text{-}Cu/Al_2O_3$ catalyst, led to no obvious change in pore size distribution. In Figure 2b, note that no pore size distribution existed in the SiO_2 supported catalysts.

3.1.3. H_2-TPR

The reduction behaviors of the Al_2O_3, SiO_2, CuO, Cu/Al_2O_3, $K\text{-}Cu/Al_2O_3$ and Cu/SiO_2, $K\text{-}Cu/SiO_2$ catalysts were studied by H_2-TPR, and the results were presented in Figure 3. No reduction peak was observed in the Al_2O_3 and SiO_2, and one reduction peak at 299 °C was clearly detected in the CuO phase. As displayed in Figure 3, the H_2-TPR profile of Cu/Al_2O_3 catalyst showed three reduction peaks at around 280, 540, and 800 °C, which corresponded to the reduction of CuO [45], $CuAl_2O_4$ [16], and $CuAlO_2$ [43], respectively. When the potassium was introduced into the catalyst, only the reduction temperature of the CuO phase in the Cu/Al_2O_3 catalyst shifted towards a higher temperature. The observed shift could be attributed to that the chemical interaction between the copper species and alumina, which was somewhat affected by the addition of potassium, in agreement with the observations of Tien-Thao et al. [40], who reported an increase in the reduction temperature of copper in Co-Cu catalysts with increasing amounts of alkali additives. The above XRD results revealed that the diffraction peaks ascribed to CuO were not observed factually for Al_2O_3 supported catalysts. It was thought that CuO particles with small size were probably dispersed on Al_2O_3 support. From Figure 3, four reduction peaks at 435, 540, 700, and 770 °C were clearly found in the Cu/SiO_2 catalyst, suggesting that four types of copper species formed on the catalyst [46]. Apparently, the addition of potassium to the Cu/SiO_2 catalyst led to no obvious change in the position of all the reduction peaks, suggesting a weak influence of potassium on the interactions between Cu and Si. In comparison of two kinds of the catalyst with different supports (in Figure 3), SiO_2 supported catalysts (Cu/SiO_2, $K\text{-}Cu/SiO_2$) showed a much narrower reduction temperature range than Al_2O_3 supported catalysts (Cu/Al_2O_3, $K\text{-}Cu/Al_2O_3$). It was easily understood that the copper oxide interacted with Al_2O_3 or SiO_2, and different supports always led to different interactions, which implied different reaction behaviors on these catalysts.

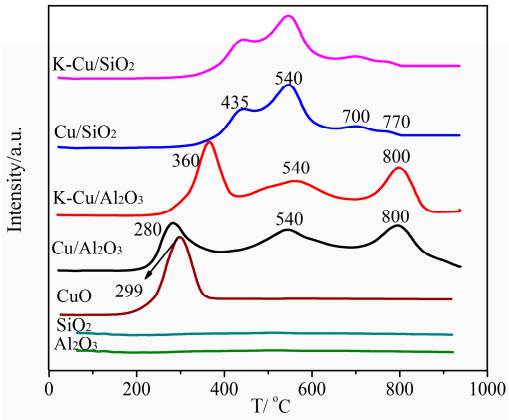

Figure 3. H_2-temperature-programmed reduction (H_2-TPR) profiles of Al_2O_3, SiO_2, CuO, Cu/Al_2O_3, K-Cu/Al_2O_3 and Cu/SiO_2, K-Cu/SiO_2 catalysts.

3.1.4. NH_3-TPD

The acidity of Cu/Al_2O_3, K-Cu/Al_2O_3 and Cu/SiO_2, K-Cu/SiO_2 catalysts was studied by NH_3-TPD measurements, and the results were shown in Figure 4. No NH_3 desorption peak was found over the CuO phase, revealing that the acid of the CuO phase was very weak. It was clearly observed that the NH_3-TPD profiles of the Al_2O_3 and Cu/Al_2O_3 catalysts were exactly the same. Specifically, two peaks at 270 and 500 °C, ascribed to the weak acidic sites and the strong acidic sites, respectively, were obviously observed in the Al_2O_3 and Cu/Al_2O_3 catalysts. These results indicated that the acid stemmed mainly from the Al_2O_3 support. When the potassium was introduced, the peak of weak acidic sites shifted to a lower temperature, and yet that of strong acidic sites slightly shifted towards a higher temperature, revealing that the strength of weak acidic sites decreased and the strength of strong acidic sites increased slightly. In comparison of the area for NH_3 desorption, it was apparent that the ammonia amounts of both weak acidic sites and strong acidic sites obviously decreased when adding the potassium, due to the partial neutralization of the surface acidity by alkali compounds [36,39,40]. As known, SiO_2 possesses remarkably weak acidity. Therefore, the present SiO_2 supported Cu catalysts (eg., Cu/SiO_2, K-Cu/SiO_2) showed no NH_3 desorption peak, with or without the potassium addition [47]. These findings indicated that the acid-base property of the prepared catalysts was closely related to the support employed, such as SiO_2 and Al_2O_3, wherein, the difference in acid-base property easily resulted in obviously different reaction behaviors.

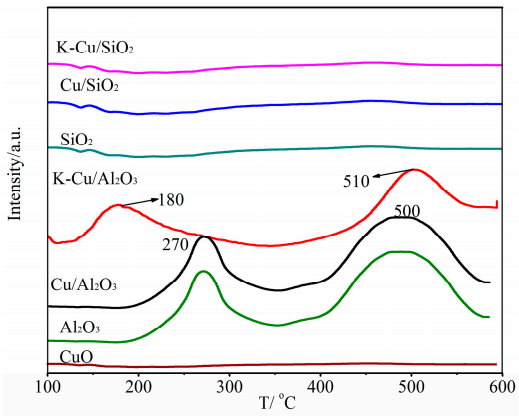

Figure 4. The temperature-programmed desorption of ammonia (NH_3-TPD) profiles of Al_2O_3, SiO_2, CuO, Cu/Al_2O_3, K-Cu/Al_2O_3 and Cu/SiO_2, K-Cu/SiO_2 catalysts.

3.1.5. XPS

XPS measurements of the representative catalysts were carried out in order to investigate the chemical state of the elements at the catalyst surface and the results were shown in Figures 5–8.

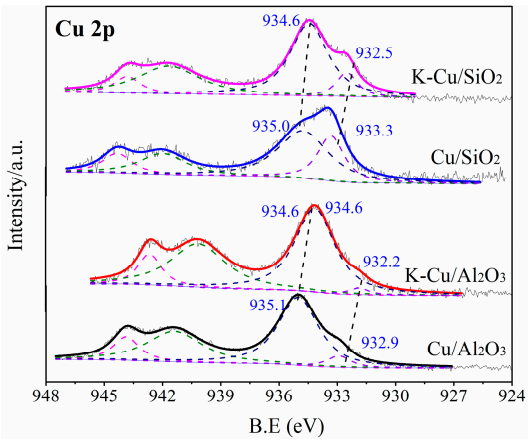

Figure 5. Cu2p$_{3/2}$ X-ray photoelectron spectroscopy (XPS) spectra of Cu/Al_2O_3, K-Cu/Al_2O_3 and Cu/SiO_2, K-Cu/SiO_2 catalysts.

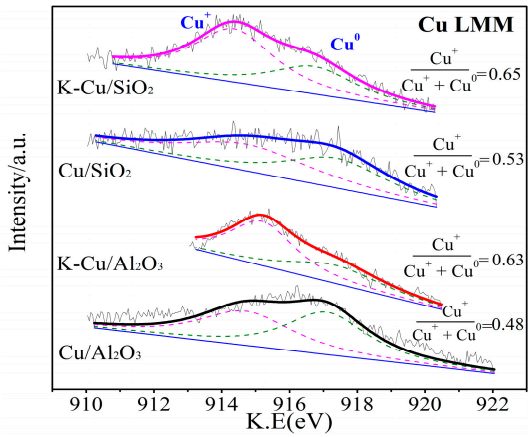

Figure 6. Cu LMM spectra of the reduced Cu/Al_2O_3, K-Cu/Al_2O_3 and Cu/SiO_2, K-Cu/SiO_2 catalysts.

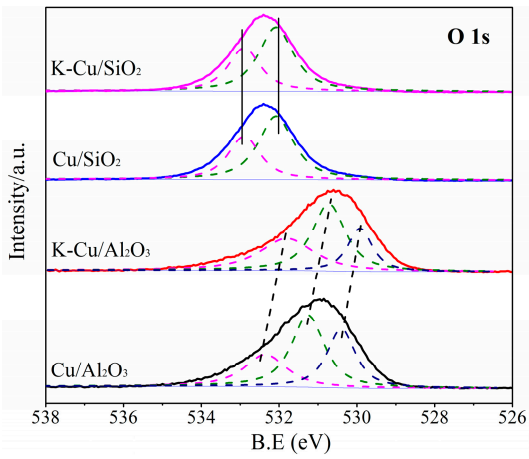

Figure 7. O1s XPS spectra of Cu/Al_2O_3, K-Cu/Al_2O_3 and Cu/SiO_2, K-Cu/SiO_2 catalysts.

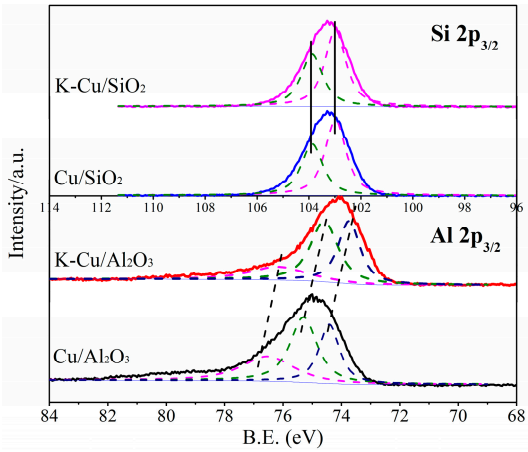

Figure 8. Al2p XPS spectra of Cu/Al_2O_3, $K\text{-}Cu/Al_2O_3$ and Si 2p XPS spectra of Cu/SiO_2, $K\text{-}Cu/SiO_2$ catalysts.

The $Cu2p_{3/2}$ binding energies (BEs) spectra of the catalysts were displayed in Figure 5. For Cu/Al_2O_3 sample, the peak appearing at ~934.0 eV, along with the shakeup satellites (940–945 eV), suggested the presence of Cu^{2+} species [30]. The asymmetry of the $Cu2p_{3/2}$ envelope could be deconvoluted into two peaks centered at around 933.0 and 935.0 eV, which were ascribed to Cu^{2+} in CuO and Cu^{2+} in $CuAl_2O_4$ respectively [16,17]. It indicated that copper oxides reacted with Al_2O_3 to form interfacial composite phases, consistent with the XRD results. When potassium was added into Cu/Al_2O_3, the peaks of the Cu^{2+} species shifted to lower BEs values. In the case of the Cu/SiO_2 catalyst, the peak (933.3 eV) of CuO and the peak (935.0 eV) of copper phyllosilicate [33,34,48] were clearly observed from Figure 5. Further, the BEs values of Cu^{2+} species shifted to the lower position with the addition of potassium. The results revealed that the chemical states of the Cu element were strongly affected by the supports employed, as well as potassium addition.

The distinction between the Cu^+ and Cu^0 species is feasible through the examination of Cu LMM XAES spectra. From the Cu LMM XAES of the reduced Cu/Al_2O_3, $K\text{-}Cu/Al_2O_3$ and Cu/SiO_2, $K\text{-}Cu/SiO_2$ catalysts shown in Figure 6, each Cu LMM spectrum contained two peaks centered at about 914–915 eV and 917–918 eV, with respect to the Cu^+ and Cu^0 species [34,48]. From the deconvolution results (inset), SiO_2 supported catalysts showed a slightly higher ratio of Cu^+ than Al_2O_3 supported catalysts. However, it was very obvious that the potassium addition induced an increase in Cu^+ species on two kinds of catalysts, which is in agreement with the observations of Lopez et al. [41].

O1s XPS spectra of Cu/Al_2O_3, $K\text{-}Cu/Al_2O_3$ and Cu/SiO_2, $K\text{-}Cu/SiO_2$ catalysts were given in Figure 7. The O1s signal of Cu/Al_2O_3 catalyst showed three overlapping peaks at around 530.1, 531.2, and 532.4 eV, indicating that three oxygen compounds formed on the catalyst surface [43]. After adding the potassium, a remarkable decrease in the BEs values was observed. However, different than the O1s XPS patterns of Al_2O_3 supported catalysts, two forms of oxygen compounds with higher BEs values were monitored over SiO_2 supported catalysts. Furthermore, the BEs values did not change with the addition of potassium. These results clearly revealed that the electronic environments of the O element on Al_2O_3 and SiO_2 supported catalysts were significantly different, and only the chemical states of the O element on the Cu/Al_2O_3 catalyst changed, apparently, by adding potassium.

Figure 8 displayed Al2p XPS spectra of Cu/Al_2O_3, $K\text{-}Cu/Al_2O_3$ and Si2p XPS spectra of Cu/SiO_2, $K\text{-}Cu/SiO_2$ catalysts. Three peaks attributed to aluminum species were obviously observed in the Cu/Al_2O_3 catalyst, revealing that three forms of aluminum species were present in this catalyst, which were related to the Al_2O_3, which formed $CuAl_2O_4$ and $CuAlO_2$, respectively [43]. The BEs values of Al2p obviously decreased when potassium was added, suggesting that the three chemical states of the Al element were affected by potassium. It was noted that two peaks centered at 103.1 and 103.9 eV were found on the Cu/SiO_2 catalyst, indicating that the Si element possessed two chemical states in the catalyst [34,48]. Also, adding potassium did not change the BEs values of Si2p. The results revealed

that the addition of the potassium promoter altered the chemical states of the Al element, while it had no influence on that of the Si element.

3.2. Catalyst Evaluation

The performances of the Cu/Al_2O_3, $K\text{-}Cu/Al_2O_3$ and Cu/SiO_2, $K\text{-}Cu/SiO_2$ catalysts for higher alcohols synthesis from syngas were presented in Table 2. It was observed that the supports, such as Al_2O_3 and SiO_2, could profoundly influence catalytic behaviors. CO conversion of 84.6% and total alcohol selectivity of 7.7%, wherein the percentages of methanol and C_{2+} alcohols were 44.0 and 56.0 wt %, respectively, were achieved over the Cu/Al_2O_3 catalyst corresponding to CO_2 selectivity of 23.0%. Conversely, the Cu/SiO_2 catalyst showed relatively low CO conversion (18.2%) and CO_2 selectivity (2.4%), but much higher total alcohol selectivity (26.7%) in spite of slight lower percentage of C_{2+} alcohols (40.3 wt %). These results indicated that the supports had obvious effects on CO conversion, CO_2 selectivity, total alcohol selectivity, and alcohol distribution.

Table 2. The performances of Cu/Al_2O_3, $K\text{-}Cu/Al_2O_3$ and Cu/SiO_2, $K\text{-}Cu/SiO_2$ catalysts.

Samples	CO Conversion (%)	STY (mg/mlcath)	Carbon Selectivity (%)				Alcohol Distribution (wt %)				
			CH_4	C_{2-5}	CO_2	ROH	MeOH	EtOH	PrOH	BuOH	$C_{5+}OH$
Cu/Al_2O_3	84.6	93.7	42.2	27.1	23.0	7.7	44.0	42.5	8.0	4.6	0.9
$K\text{-}Cu/Al_2O_3$	48.5	141.4	23.2	19.5	32.5	24.1	34.9	38.3	16.2	8.5	2.0
Cu/SiO_2	18.2	49.5	42.3	28.3	2.4	26.7	59.8	34.6	4.5	1.1	0.1
$K\text{-}Cu/SiO_2$	16.8	55.0	27.4	27.7	16.1	28.8	51.8	32.6	9.8	4.4	1.4

Reaction conditions: 10 MPa, 400 °C, 5000 h^{-1}.

Further, one could observe from Table 2 that the potassium addition induced obviously different reaction behaviors over the Al_2O_3 and SiO_2 supported catalysts. Seemingly, for Al_2O_3 supported catalysts, the potassium addition resulted in a dramatic decrease in CO conversion, CH_4 selectivity, and C_{2-5} hydrocarbons selectivity (from 84.6 to 48.5%, from 42.2 to 23.2%, and from 27.1 to 19.5%, respectively) but an obvious increase in CO_2 selectivity and total alcohol selectivity (from 23.0 to 32.5% and from 7.7 to 24.1%, respectively). Besides, the $K\text{-}CuO/Al_2O_3$ showed a relatively lower selectivity to methanol but a higher one to C_{2+} alcohols, indicating that alcohol chain-growth was enhanced. Chain-growth probabilities (α) of alcohols were calculated, as shown in Figure 9. In the case of SiO_2 supported catalysts, the change trend in the CH_4 selectivity, CO_2 selectivity, and alcohol chain-growth, induced by potassium addition, was similar with that in Al_2O_3 supported catalysts. Whereas, different than the Cu/Al_2O_3 catalyst, adding the potassium into the Cu/SiO_2 catalyst did not significantly change the values of CO conversion (~17.0%), total alcohol selectivity (~27.0%), and C_{2-5} hydrocarbons selectivity (~28.0%). Conclusively, potassium introduction did not only promote the formation of CO_2 and inhibit the CH_4 formation, but also enhanced the carbon chain growth probability of products; moreover, the potassium had a greater impact on the CO conversion, total alcohol selectivity, and C_{2-5} hydrocarbons selectivity over the Al_2O_3 supported catalysts than that over SiO_2 supported catalysts.

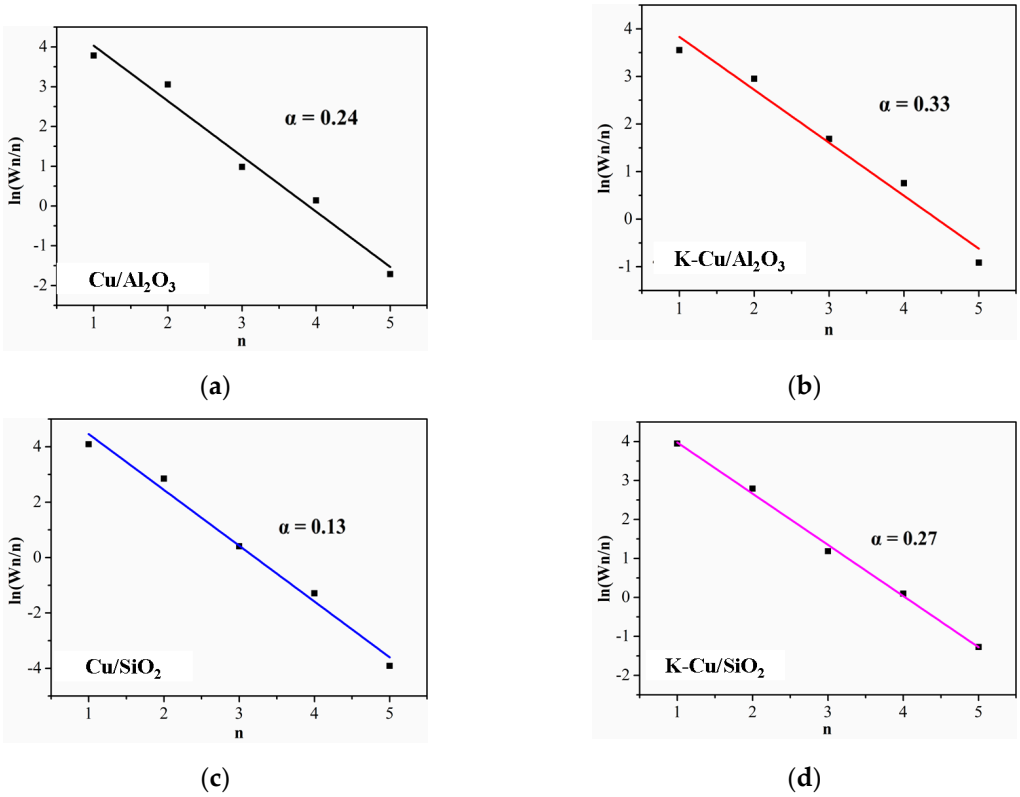

Figure 9. Anderson-Schulz-Flory (A-S-F) plots for the distribution of alcohols for catalysts: (**a**) Cu/Al_2O_3, (**b**) K-Cu/Al_2O_3 and (**c**) Cu/SiO_2, (**d**) K-Cu/SiO_2. $Wn = n \times (1 - \alpha)^2 \times \alpha^{n-1}$, where Wn stands for the mass fraction of alcohols containing n carbon atoms.

3.3. In Situ FTIR

To further obtain detailed information on the molecular events that occur on the surface of the catalyst, CO adsorption over reduced Cu/Al_2O_3, K-Cu/Al_2O_3 and Cu/SiO_2, K-Cu/SiO_2 catalysts was monitored using in situ FTIR. As displayed in Figure 10, there were two absorption bands in the region of 3200–2850 cm^{-1} (ν C-H) and 1650–1300 cm^{-1} (ν COO) observed, assigned to the adsorbed hydrocarbons and formate species (C1 oxygenate species), respectively [49,50]. For the Cu/Al_2O_3 catalyst, very weak peaks at 1650–1300 cm^{-1} were detected, revealing the presence of only a trace of C1 oxygenate species on the catalyst surface, which were approved to contribute to the formation of higher alcohols [2,41,50]. It was also noted that the peaks at around 3200–2850 cm^{-1}, ascribed to the hydrogenation, was strong on the Cu/Al_2O_3 catalyst. When potassium was added, the band peaks of the C1 oxygenate species obviously increased, whereas the intensity of hydrocarbons decreased. As Santos et al. [2] reported, potassium, in close vicinity to an adsorbed methyl group, stabilized oxygenate species that were found to play an important role in the syngas to alcohol route. Thus, the reaction shifted towards alcohols, rather than hydrocarbons, when potassium modified the Cu/Al_2O_3 catalyst. When SiO_2 was used as support, it was noted that the peak at 1650–1300 cm^{-1} ascribed to the C1 oxygenate species was enhanced on the Cu/SiO_2 catalyst, which was very different with that of Cu/Al_2O_3 catalyst, on which only trace amounts of the C1 oxygenate species were formed (Figure 10); moreover, it seemed that adding potassium had no effect on the amount of C1 oxygenate species formed. This explained why the Cu/SiO_2 and K-Cu/SiO_2 catalysts exhibited the similar alcohol selectivity of ~27% (Table 2).

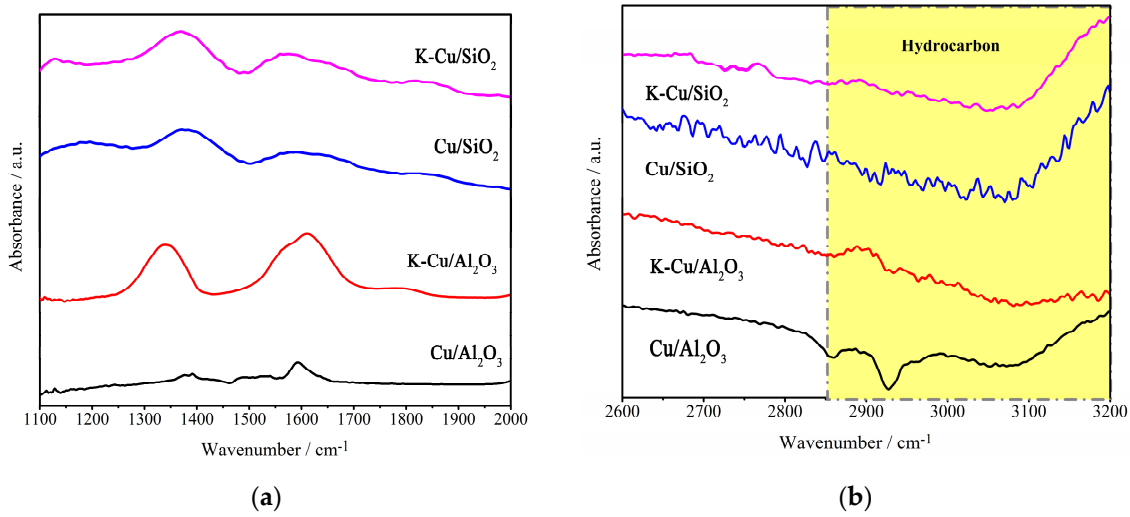

Figure 10. In situ Fourier-transform infrared (FTIR) spectra of CO adsorption over reduced Cu/Al_2O_3, $K\text{-}Cu/Al_2O_3$ and Cu/SiO_2, $K\text{-}Cu/SiO_2$ catalysts during CO flow at 400 °C for 30 min and then under Ar at 400 °C for 30 min.

3.4. Discussion

The results obtained by the test and characterizations of Cu/Al_2O_3 and Cu/SiO_2 samples clearly demonstrated that the physicochemical properties and catalytic performances of the Cu-based catalyst were strongly affected by the types of supports employed (Al_2O_3, SiO_2). In comparison to the Cu/Al_2O_3 catalyst with only 7.7% of total alcohol selectivity, the Cu/SiO_2 catalyst possessed a much higher total alcohol selectivity of 26.7%. As confirmed by the FTIR result, only a trace of the C1 oxygenate species was detected on the Cu/Al_2O_3 catalyst, but a relatively large amount of the C1 oxygenate species existed on the surface of the Cu/SiO_2 catalyst. Some authors have pointed out that the oxygenate species played an essential role in directing the synthesis toward alcohols, rather than hydrocarbons [39–41,50,51]. Zhang et al. [52,53] conducted a series of DFT studies to assess the mechanism of CO hydrogenation to higher alcohols on Cu (110) [52] and Cu (211) [53], and pointed out that the CH_xO species as key intermediates for higher alcohols synthesis could give the CH_x species through the C-O cleavage, and CH_x monomers subsequently combined with CO or CHO to form alcohol. Based on the above, it was apparent that the more adsorbed C1 oxygenate species on the Cu/SiO_2 catalyst inevitably resulted in an increase in the concentration of CH_x species via the C-O cleavage, and, finally, promoted the formation of alcohol. Hence, the Cu/SiO_2 catalyst with a higher amount of the C1 oxygenate species exhibited a higher total alcohols selectivity than the Cu/Al_2O_3 catalyst. Further, by comparing to the Cu/SiO_2 catalyst, the Cu/Al_2O_3 catalyst showed higher selectivities towards C_{2+} alcohols. As reported [54–56], aldol condensation as one of the key steps for carbon-chain growth of alcohol products easily proceeded on basic oxide catalysts or acid oxide catalysts. The NH_3-TPD result revealed that the surface acidity of the Cu/Al_2O_3 catalyst was much stronger than that of the Cu/SiO_2 catalyst. Therefore, the possibility of carbon-chain growth occurred on the acid Cu/Al_2O_3 catalyst more easily. Despite that the ethanol selectivities were both 32.6 wt % above on Al_2O_3 and SiO_2-supported catalysts, which was probably due to high $Cu^+/(Cu^++Cu^0)$ values, Cu/SiO_2 with a relatively high $Cu^+/(Cu^++Cu^0)$ value did not give higher ethanol selectivity than Cu/Al_2O_3. Our previous work [16,17] has demonstrated that the amounts of Cu^+ species were somewhat responsible for the formation of ethanol. These results suggested that the ethanol formation was affected by many factors, such as $Cu^+/(Cu^++Cu^0)$ value, the physical properties, the reduction behaviors, acidity, and electronic properties on the catalyst, which are synergetic.

In addition, CO conversion and CO_2 selectivity of the Cu/Al_2O_3 catalyst also showed significant differences from that of the Cu/SiO_2 catalyst. As revealed by the XRD and H_2-TPR results, although

the refractory phases formed over Al_2O_3 or SiO_2 supported Cu catalysts under 900 °C, the two kinds of the catalysts with different supports presented differences in the types of copper species and the reduction behaviors of copper species. N_2 absorption-desorption results indicated that the textural parameters of the Cu/Al_2O_3 and Cu/SiO_2 catalysts, despite uncalcined supports with similar surface areas (157–160 m^2/g), were significantly different. Furthermore, the Cu/Al_2O_3 catalyst with a type IV adsorption isotherm showed a wide pore size distribution, but the Cu/SiO_2 catalyst had no N_2 adsorption-desorption isotherms and pore size distribution. The NH_3-TPD result suggested that the acidity was obviously detected in the Cu/Al_2O_3 catalyst, but no acidity was observed in the Cu/SiO_2 catalyst. Moreover, the XPS results showed that the Cu, O elements of the Cu/Al_2O_3 catalyst differed from that of the Cu/SiO_2 catalyst in electronic environments. As confirmed by the FTIR result, only a trace of C1 oxygenate species, contributing to alcohols formation, was detected on the Cu/Al_2O_3 catalyst, while a relatively large amount of C1 oxygenate species existed on the surface of the Cu/SiO_2 catalyst. These characterization results indicated that the structural and chemical properties of Cu/Al_2O_3 and Cu/SiO_2 catalysts showed obvious differences and thus affected the catalytic behaviors of the catalysts synergistically.

The performances of two kinds of catalysts with the support employed, such as SiO_2 and Al_2O_3, were also significantly affected by the potassium introduction. Doping potassium into the Al_2O_3 and SiO_2 supported catalysts improved the carbon chain growth probability of alcohol products. This was probably because potassium introduction provided new basic sites for the aldol condensation of lower alcohols to higher alcohols [40,57]. Moreover, alkali elements are known to be good promoters for the WGS reaction ($CO + H_2O \rightarrow CO_2 + H_2$) when introduced at optimum content [9,15,39,50]. As a result, the addition of potassium to Cu/Al_2O_3 and Cu/SiO_2 catalysts resulted in the improvement of CO_2 formation.

Additionally, according to the test results, doping potassium into Cu/Al_2O_3 and Cu/SiO_2 catalysts induced distinct differences in the total alcohol selectivity. For Al_2O_3 supported catalysts, total alcohol selectivity increased up to 24.1 from previous 7.7%, clearly, when the potassium was added. It indicated that the presence of potassium promoted the formation of alcohols. As confirmed by the FTIR result, by adding the K promoter, the relative amount of adsorbed C1 oxygenate species, as intermediates in higher alcohols synthesis [41,50], increased obviously by tuning the reduction behavior, neutralizing the surface acidity, and altering of the electronic properties, whereas the formation of hydrocarbons (mainly CH_4 and C_{2-5} hydrocarbons) was severely inhibited [39,50]. Anton et al. [39–41] reported that alkali (K/Cs/Rb) modified Cu-based catalysts can enhance the stability of CHx intermediate species. Therefore, total alcohols selectivity on the K-Cu/Al_2O_3 catalyst increased dramatically with potassium introduction. However, for the SiO_2 supported catalyst, the potassium addition hardly had an obvious effect on the relative amount of C1 oxygenate species, thus the total alcohol selectivity on K-Cu/SiO_2 catalyst remained almost unchanged. Due to very weak acidity of the SiO_2 supported catalyst, only CH_4 selectivity decreased sharply after potassium introduction, implying that potassium addition more preferentially inhibited CH_4 formation, compared with that of C_{2-5} hydrocarbons. Obviously, potassium addition could somehow modify the structural and chemical properties of the Cu/Al_2O_3 catalyst and enhance the amount of C1 oxygenate species, which narrowed the gap in performances of the two Al_2O_3 and SiO_2 supported catalysts.

4. Conclusions

In this work, the Al_2O_3 and SiO_2 supported Cu catalysts prepared by a facile impregnation method were used for higher alcohols synthesis from CO hydrogenation. Based on the remarkably different reaction behaviors over the Cu catalysts supported on Al_2O_3 and SiO_2, some systematical investigations were carried out to understand the main reasons. The Cu/SiO_2 catalyst possessed a higher amount of the C1 oxygenate species and showed higher total alcohols selectivity than the Cu/Al_2O_3 catalyst. Compared to the very weak acidity of the SiO_2 supported catalyst, the carbon chain growth probability of alcohol products occurred on the acid Cu/Al_2O_3 catalyst more easily.

Further, the Cu/Al_2O_3 and Cu/SiO_2 catalysts showed obvious differences in the structural and physicochemical properties, such as the types of copper species, the reduction behaviors, acidity, and electronic properties. As a result, the CO conversion, alcohol distribution, and CO_2 selectivity of the Cu/Al_2O_3 catalyst were different from that of the Cu/SiO_2 catalyst. Additionally, the performances of the Cu catalysts supported on Al_2O_3 and SiO_2 became more similar when the potassium was introduced. Wherein, the potassium was approved to modify the structural and chemical properties of the catalysts to some extent.

Author Contributions: The idea was conceived by Y.T. and X.L.; X.L. performed the experiments and drafted the paper under the supervision of Y.T. and J.Z.; M.Z. (Min Zhang), W.Z., M.Z. (Meng Zhang), H.X. and Y.W. helped to collect and analyse some characterization data. The manuscript was revised and checked through the comments of all authors. All authors have given approval for the final version of the manuscript.

Funding: This research was funded by the National Natural Science Foundation of China (No. 21573269), the Key Research and Development Program of Shanxi Province (No. MD2014-10).

Acknowledgments: The authors thank the financial support of National Natural Science Foundation of China (No. 21573269), the Key Research and Development Program of Shanxi Province (No. MD2014-10).

Conflicts of Interest: The authors declare no conflict of interest.

References

1. Yang, Y.; Qi, X.; Wang, X.; Lv, D.; Yu, F.; Zhong, L.; Wang, H.; Sun, Y.H. Deactivation study of CuCo catalyst for higher alcohol synthesis via syngas. *Catal. Today* **2016**, *270*, 101–107. [CrossRef]
2. Santos, V.P.; van der Linden, B.; Chojecki, A.; Budroni, G.; Corthals, S.; Shibata, H.; Meima, G.R.; Kapteijn, F.; Makkee, M.; Gascon, J. Mechanistic Insight into the Synthesis of Higher Alcohols from Syngas: The Role of K Promotion on MoS_2 Catalysts. *ACS Catal.* **2013**, *3*, 1634–1637. [CrossRef]
3. Goldemberg, J. Ethanol for a sustainable energy future. *Science* **2007**, *315*, 808–810. [CrossRef]
4. Luk, H.T.; Mondelli, C.; Ferré, D.C.; Stewart, J.A.; Pérez-Ramírez, J. Status and prospects in higher alcohols synthesis from syngas. *Chem. Soc. Rev.* **2017**, *46*, 1358–1426. [CrossRef]
5. Zhang, R.; Duan, T.; Wang, B.J.; Ling, L.X. Unraveling the role of support surface hydroxyls and its effect on the selectivity of C2 species over $Rh/\gamma\text{-}Al_2O_3$ catalyst in syngas conversion: A theoretical study. *Appl. Surf. Sci.* **2016**, *379*, 384–394. [CrossRef]
6. Choi, Y.; Liu, P. Mechanism of ethanol synthesis from syngas on Rh (111). *J. Am. Chem. Soc.* **2009**, *131*, 13054–13061. [CrossRef]
7. Gao, W.; Zhao, Y.F.; Liu, J.M.; Huang, Q.W.; He, S.; Li, C.M.; Zhao, J.W.; Wei, M. Catalytic conversion of syngas to mixed alcohols over CuFe-based catalysts derived from layered double hydroxides. *Catal. Sci. Technol.* **2013**, *3*, 1324–1332. [CrossRef]
8. Xiao, K.; Qi, X.Z.; Bao, Z.H.; Wang, X.X.; Zhong, L.S.; Fang, K.G.; Lin, M.G.; Sun, Y.H. CuFe, CuCo and CuNi nanoparticles as catalysts for higher alcohol synthesis from syngas: a comparative study. *Catal. Sci. Technol.* **2013**, *3*, 1591–1602. [CrossRef]
9. Zaman, S.F.; Pasupulety, N.; Al-Zahrani, A.A.; Daous, M.A.; Al-Shahrani, S.; Driss, H.; Petrov, L.A. Carbon monoxide hydrogenation on potassium promoted Mo_2N catalysts. *Appl. Catal. A Gen.* **2017**, *532*, 133–145. [CrossRef]
10. Wang, P.; Bai, Y.X.; Xiao, H.; Tian, S.P.; Zhang, Z.Z.; Wu, Y.Q.; Xie, H.J.; Yang, G.H.; Han, Y.Z.; Tan, Y.S. Effect of the dimensions of carbon nanotube channels on copper-cobalt-cerium catalysts for higher alcohols synthesis. *Catal. Commun.* **2016**, *75*, 92–97. [CrossRef]
11. Wang, P.; Zhang, J.F.; Bai, Y.X.; Xiao, H.; Tian, S.P.; Xie, H.J.; Yang, G.H.; Tsubaki, N.; Han, Y.Z.; Tan, Y.S. Ternary copper-cobalt-cerium catalyst for the production of ethanol and higher alcohols through CO hydrogenation. *Appl. Catal. A Gen.* **2016**, *514*, 14–23. [CrossRef]
12. Wang, P.; Chen, S.Y.; Bai, Y.X.; Gao, X.F.; Li, X.L.; Sun, K.; Xie, H.J.; Yang, G.H.; Han, Y.Z.; Tan, Y.S. Effect of the promoter and support on cobalt-based catalysts for higher alcohols synthesis through CO hydrogenation. *Fuel* **2017**, *195*, 69–81. [CrossRef]

13. Sun, J.; Cai, Q.X.; Wan, Y.; Wan, S.L.; Wang, L.; Lin, J.D.; Mei, D.H.; Wang, Y. Promotional effects of cesium promoter on higher alcohol synthesis from syngas over cesium-promoted $Cu/ZnO/Al_2O_3$ catalysts. *ACS Catal.* **2016**, *6*, 5771–5785. [CrossRef]
14. Liu, G.L.; Niu, T.; Cao, A.; Geng, Y.X.; Zhang, Y.; Liu, Y. The deactivation of Cu-Co alloy nanoparticles supported on ZrO_2 for higher alcohols synthesis from syngas. *Fuel* **2016**, *176*, 1–10. [CrossRef]
15. Gupta, M.; Smith, M.L.; Spivey, J.J. Heterogeneous catalytic conversion of dry syngas to ethanol and higher alcohols on Cu-based catalysts. *ACS Catal.* **2011**, *1*, 641–656. [CrossRef]
16. Li, X.L.; Zhang, Q.D.; Xie, H.J.; Gao, X.F.; Wu, Y.Q.; Yang, G.H.; Wang, P.; Tian, S.P.; Tan, Y.S. Facile preparation of Cu-Al oxide catalysts and their application in the direct synthesis of ethanol from syngas. *Chem. Select* **2017**, *2*, 10365–10370. [CrossRef]
17. Li, X.L.; Xie, H.J.; Gao, X.F.; Wu, Y.Q.; Wang, P.; Tian, S.P.; Zhang, T.; Tan, Y.S. Effects of calcination temperature on structure-activity of $K\text{-}ZrO_2/Cu/Al_2O_3$ catalysts for ethanol and isobutanol synthesis from CO hydrogenation. *Fuel* **2018**, *227*, 199–207. [CrossRef]
18. Sun, K.; Gao, X.F.; Bai, Y.X.; Tan, M.H.; Yang, G.H.; Tan, Y.S. Synergetic catalysis of bimetallic copper-cobalt nanosheets for direct synthesis of ethanol and higher alcohols from syngas. *Catal. Sci. Technol.* **2018**, *8*, 3936–3947. [CrossRef]
19. Liakakou, E.T.; Heracleous, E.; Triantafyllidis, K.S.; Lemonidou, A.A. K-promoted NiMo catalysts supported on activated carbon for the hydrogenation reaction of CO to higher alcohols: Effect of support and active metal. *Appl. Catal. B Environ.* **2015**, *165*, 296–305. [CrossRef]
20. Wang, J.J.; Chernavskii, P.A.; Khodakov, A.Y. Influence of the support and promotion on the structure and catalytic performance of copper-cobalt catalysts for carbon monoxide hydrogenation. *Fuel* **2013**, *103*, 1111–1122. [CrossRef]
21. Wang, J.J.; Chernavskii, P.A.; Khodakov, A.Y.; Wang, Y. Structure and catalytic performance of alumina-supported copper–cobalt catalysts for carbon monoxide hydrogenation. *J. Catal.* **2012**, *286*, 51–61. [CrossRef]
22. Ding, J.; Popa, T.; Tang, J.; Gasem, K.A.M.; Fan, M.; Zhong, Q. Highly selective and stable Cu/SiO_2 catalysts prepared with a green method for hydrogenation of diethyl oxalate into ethylene glycol. *Appl. Catal. B Environ.* **2017**, *209*, 530–542. [CrossRef]
23. Lee, J.H.; Reddy, K.H.; Jung, J.S.; Yang, E.; Moon, D.J. Role of support on higher alcohol synthesis from syngas. *Appl. Catal. A Gen.* **2014**, *480*, 128–133. [CrossRef]
24. Schumann, J.; Eichelbaum, M.; Lunkenbein, T.; Thomas, N.; Álvarez Galván, M.C.; Schlögl, R.; Behrens, M. Promoting strong metal support interaction: Doping ZnO for enhanced activity of Cu/ZnO:M (M = Al, Ga, Mg) catalysts. *ACS Catal.* **2015**, *5*, 3260–3270. [CrossRef]
25. Schneider, J.; Struve, M.; Trommler, U.; Schlüter, M.; Seidel, L.; Dietrich, S.; Rönsch, S. Performance of supported and unsupported Fe and Co catalysts for the direct synthesis of light alkenes from synthesis gas. *Fuel Process. Technol.* **2018**, *170*, 64–78. [CrossRef]
26. Kim, T.W.; Kleitz, F.; Jun, J.W.; Chae, H.J.; Kim, C.U. Catalytic conversion of syngas to higher alcohols over mesoporous perovskite catalysts. *J. Ind. And Eng. Chem.* **2017**, *51*, 196–205. [CrossRef]
27. Liu, Y.J.; Deng, X.; Han, P.D.; Huang, W. CO hydrogenation to higher alcohols over CuZnAl catalysts without promoters: Effect of pH value in catalyst preparation. *Fuel Process. Technol.* **2017**, *167*, 575–581. [CrossRef]
28. París, R.S.; Montes, V.; Boutonnet, M.; Järås, S. Higher alcohol synthesis over nickel-modified alkali-doped molybdenum sulfide catalysts prepared by conventional coprecipitation and coprecipitation in microemulsions. *Catal. Today* **2015**, *258*, 294–303. [CrossRef]
29. Song, Z.Y.; Shi, X.P.; Ning, H.Y.; Liu, G.L.; Zhong, H.X.; Liu, Y. Loading clusters composed of nanoparticles on ZrO_2 support via a perovskite-type oxide of $La_{0.95}Ce_{0.05}Co_{0.7}Cu_{0.3}O_3$ for ethanol synthesis from syngas and its structure variation with reaction time. *Appl. Surf. Sci.* **2017**, *405*, 1–12. [CrossRef]
30. Choi, S.M.; Kang, Y.J.; Kim, S.W. Effect of γ-alumina nanorods on CO hydrogenation to higher alcohols over lithium-promoted CuZn-based catalysts. *Appl. Catal. A Gen.* **2018**, *549*, 188–196. [CrossRef]
31. Jiang, Y.; Yang, H.Y.; Gao, P.; Li, X.P.; Zhang, J.M.; Liu, H.J.; Wang, H.; Wei, W.; Sun, Y.H. Slurry methanol synthesis from CO_2 hydrogenation over micro-spherical SiO_2 support Cu/ZnO catalysts. *J. CO_2 Util.* **2018**, *26*, 642–651. [CrossRef]

32. Su, J.J.; Zhang, Z.P.; Fu, D.L.; Liu, D.; Xu, X.C.; Shi, B.F.; Wang, X.; Si, R.; Jiang, Z.; Xu, J.; Han, Y.F. Higher alcohols synthesis from syngas over $CoCu/SiO_2$ catalysts: Dynamic structure and the role of Cu. *J. Catal.* **2016**, *336*, 94–106. [CrossRef]
33. Huang, X.M.; Ma, M.; Miao, S.; Zheng, Y.P.; Chen, M.S.; Shen, W.J. Hydrogenation of methyl acetate to ethanol over a highly stable Cu/SiO_2 catalyst: Reaction mechanism and structural evolution. *Appl. Catal. A Gen.* **2017**, *531*, 79–88. [CrossRef]
34. Ye, R.P.; Lin, L.; Yang, J.X.; Sun, M.L.; Li, F.; Li, B.; Yao, Y.G. A new low-cost and effective method for enhancing the catalytic performance of Cu-SiO_2 catalysts for the synthesis of ethylene glycol via the vapor-phase hydrogenation of dimethyl oxalate by coating the catalysts with dextrin. *J. Catal.* **2017**, *350*, 122–132. [CrossRef]
35. Li, X.L.; Yang, G.H.; Zhang, M.; Gao, X.F.; Xie, H.J.; Bai, Y.X.; Wu, Y.Q.; Pan, J.X.; Tan, Y.S. Insight into the correlation between Cu species evolution and ethanol selectivity in the direct ethanol synthesis from CO hydrogenation. *ChemCatChem* **2018**, *11*, 1123–1130. [CrossRef]
36. Cosultchi, A.; Pérez-Luna, M.; Morales-Serna, J.A.; Salmón, M. Characterization of modified Fischer-Tropsch catalysts promoted with alkaline metals for higher alcohol synthesis. *Catal. Lett.* **2012**, *142*, 368–377. [CrossRef]
37. Tan, L.; Yang, G.H.; Yoneyama, Y.; Kou, Y.L.; Tan, Y.S.; Vitidsant, T. Iso-butanol direct synthesis from syngas over the alkali metals modified Cr/ZnO catalysts. *Appl. Catal. A Gen.* **2015**, *505*, 141–149. [CrossRef]
38. Sun, J.; Wan, S.; Wang, F.; Lin, J.D.; Wang, Y. Selective synthesis of methanol and higher alcohols over $Cs/Cu/ZnO/Al_2O_3$ catalysts. *Ind. Eng. Chem. Res.* **2015**, *54*, 7841–7851. [CrossRef]
39. Anton, J.; Nebel, J.; Song, H.Q.; Froese, C.; Weide, P.; Ruland, H.; Muhler, M.; Kaluza, S. The effect of sodium on the structure-activity relationships of cobalt-modified $Cu/ZnO/Al_2O_3$ catalysts applied in the hydrogenation of carbon monoxide to higher alcohols. *J. Catal.* **2016**, *335*, 175–186. [CrossRef]
40. Tien-Thao, N.; Zahedi-Niaki, M.H.; Alamdari, H.; Kaliaguine, S. Effect of alkali additives over nanocrystalline Co-Cu-based perovskites as catalysts for higher-alcohol synthesis. *J. Catal.* **2007**, *245*, 348–357. [CrossRef]
41. Lopez, L.; Montes, V.; Kusar, H.; Cabrera, S.; Boutonnet, M.; Järås, S. Syngas conversion to ethanol over a mesoporous Cu/MCM-41 catalyst: Effect of K and Fe promoters. *Appl. Catal. A Gen.* **2016**, *526*, 77–83. [CrossRef]
42. Yang, Q. Synthesis of γ-Al_2O_3 nanowires through a boehmite precursor route. *Bull. Mater. Sci.* **2011**, *34*, 239. [CrossRef]
43. Kato, S.; Fujimaki, R.; Ogasawara, M.; Wakabayashi, T.; Nakahara, Y.; Nakata, S. Oxygen storage capacity of $CuMO_2$ (M = Al, Fe, Mn, Ga) with a delafossite-type structure. *Appl. Catal. B Environ.* **2009**, *89*, 183–188. [CrossRef]
44. Tada, S.H.; Watanabe, F.; Kiyota, K.; Shimoda, N.; Hayashi, R.; Takahashi, M.; Nariyuki, A.; Igarashi, A.; Satokawa, S. Ag addition to CuO-ZrO_2 catalysts promotes methanol synthesis via CO_2 hydrogenation. *J. Catal.* **2017**, *351*, 107–118. [CrossRef]
45. Li, M.M.J.; Zeng, Z.Y.; Liao, F.L.; Hong, X.L.; Tsang, S.C.E. Enhanced CO_2 hydrogenation to methanol over CuZn nanoalloy in Ga modified Cu/ZnO catalysts. *J. Catal.* **2016**, *343*, 157–167. [CrossRef]
46. Wang, B.; Cui, Y.Y.; Wen, C.; Chen, X.; Dong, Y.; Dai, W.L. Role of copper content and calcination temperature in the structural evolution and catalytic performance of Cu/P25 catalysts in the selective hydrogenation of dimethyl oxalate. *Appl. Catal. A Gen.* **2016**, *509*, 66–74. [CrossRef]
47. Soled, S. Silica-supported catalysts get a new breath of life. *Science* **2015**, *350*, 1171–1172. [CrossRef] [PubMed]
48. Liu, Y.T.; Ding, J.; Bi, J.C.; Sun, Y.P.; Zhang, J.; Liu, K.F.; Kong, F.H.; Xiao, H.C.; Chen, J.G. Effect of Cu-doping on the structure and performance of molybdenum carbide catalyst for low-temperature hydrogenation of dimethyl oxalate to ethanol. *Appl. Catal. A Gen.* **2017**, *529*, 143–155. [CrossRef]
49. Kwak, G.; Woo, M.H.; Kang, S.C.; Park, H.G.; Lee, Y.J.; Jun, K.W.; Ha, K.S. In situ monitoring during the transition of cobalt carbide to metal state and its application as Fischer-Tropsch catalyst in slurry phase. *J. Catal.* **2013**, *307*, 27–36. [CrossRef]
50. Claure, M.T.; Chai, S.H.; Dai, S.; Unocic, K.A.; Alamgir, F.M.; Agrawal, P.K.; Jones, C.W. Tuning of higher alcohol selectivity and productivity in CO hydrogenation reactions over K/MoS_2 domains supported on mesoporous activated carbon and mixed MgAl oxide. *J. Catal.* **2015**, *324*, 88–97. [CrossRef]

51. Tian, S.P.; Wang, S.C.; Wu, Y.Q.; Gao, J.W.; Wang, P.; Xie, H.J.; Yang, G.H.; Han, Y.Z.; Tan, Y.S. The role of potassium promoter in isobutanol synthesis over Zn-Cr based catalysts. *Catal. Sci. Technol.* **2016**, *6*, 4105–4115. [CrossRef]
52. Zhang, R.; Sun, X.; Wang, B. Insight into the Preference Mechanism of CHx (x = 1-3) and C-C Chain Formation Involved in C2 Oxygenate Formation from Syngas on the Cu (110) Surface. *J. Phys. Chem. C* **2013**, *117*, 6594–6606. [CrossRef]
53. Zhang, R.; Wang, G.; Wang, B. Insights into the mechanism of ethanol formation from syngas on Cu and an expanded prediction of improved Cu-based catalyst. *J. Catal.* **2013**, *305*, 238–255. [CrossRef]
54. Zhang, J.F.; Zhang, M.; Wang, X.X.; Zhang, Q.D.; Song, F.E.; Tan, Y.S.; Han, Y.Z. Direct synthesis of isobutyraldehyde from methanol and ethanol on Cu-Mg/Ti-SBA-15 catalysts: the role of Ti. *New J. Chem.* **2017**, *41*, 9639–9648. [CrossRef]
55. Zhang, J.F.; Wu, Y.Q.; Li, L.; Wang, X.X.; Zhang, Q.D.; Zhang, T.; Tan, Y.S.; Han, Y.Z. Ti-SBA-15 supported Cu-MgO catalyst for synthesis of isobutyraldehyde from methanol and ethanol. *RSC Adv.* **2016**, *6*, 85940–85950. [CrossRef]
56. Wu, Y.Q.; Xie, H.J.; Tian, S.P.; Tsubaki, N.; Han, Y.Z.; Tan, Y.S. Isobutanol synthesis from syngas over K-Cu/ZrO_2-$La_2O_{3(x)}$ catalysts: effect of La-loading. *J. Mol. Catal. A Chem.* **2015**, *396*, 254–260. [CrossRef]
57. Heracleous, E.; Liakakou, E.T.; Lappas, A.A.; Lemonidou, A.A. Investigation of K-promoted Cu-Zn-Al, Cu-X-Al and Cu-Zn-X (X= Cr, Mn) catalysts for carbon monoxide hydrogenation to higher alcohols. *Appl. Catal. A Gen.* **2013**, *455*, 145–154. [CrossRef]